HETEROCYCLES, Vol. 100, No. 9, 2020, pp. 1426 - 1440. © 2020 The Japan Institute of Heterocyclic Chemistry
Received, 29th May, 2020, Accepted, 6th July, 2020, Published online, 15th July, 2020
DOI: 10.3987/COM-20-14293

STRUCTURAL AND DFT STUDY OF 1-(3-AMINO-1,4-DIOXO-1,4-DIHYDRONAPHTHALEN-2-YL)-3,4-DICHLORO-1*H*-PYRROLE-2,5-DIONE: HYPOTHESIS FOR THE RING CLOSURE

Bader A. Salameh[1]* and Murad A. AlDamen[2]*

[1] Department of Chemistry, Faculty of Science, the Hashemite University, Zarqa 13133, Jordan. [2] Department of Chemistry, School of Science, the University of Jordan, Amman 11942, Jordan. Email: bader@hu.edu.jo, maldamen@ju.edu.jo

Abstract – The reaction of 2,3-dichloromaleic anhydride with 2,3-diamino-1,4-naphthoquinone was studied and afforded to 1-(3-amino-1,4-dioxo-1,4-dihydronaphthalen-2-yl)-3,4-dichloro-1*H*-pyrrole-2,5-dione (**3**). Experimental techniques (NMR and single-crystal structures) confirmed the structure of **3**. The study was extended to explore the failure of the intramolecular cyclization of **3** to the imidazole ring. Density Functional Theory at level B3LYP/6-31G(d,p) of theory were used to examine the optimized molecular geometry and to understand the reaction mechanism which reveals that the failure of cyclization is possibly due to positive charge of the amine in addition to the high repulsion between the naphthoquinone and the maleimide oxygens.

INTRODUCTION

Imidazoles and benzimidazoles are among the most studied heterocycles in the azole family, mainly due to their well-known biological activities, which include but not limited to antitumor, anti-bacterial, anti-fungus, anti-viral, anti-ulcer and anti-hypertensive compounds.[1-3] Derivatization of benzimidazole on positions 1 or 2 exhibits favorable biological responses according to several studies.[3-5] In contrast of that, there are only a few reports that deal with the naphthoquinone analogous of benzimidazole where naphthoquinone is fused to imidazole ring, despite the well-known pharmacological properties of naphthoquinone derivatives which include antitumor, wound healing, anti-inflammatory, anti-parasitic, anti-bacterial, anti-fungal, anti-viral, insecticidal, antipyretic and cytotoxic activities.[6,7] Benzimidazoles were prepared by different methods, one particular method we want to focus on was a reaction that gave unique derivatives of benzimidazole in which the derivatization took place on positions 1 and 2 on the benzimidazole nucleus. That reaction was through the condensation of an *o*-phenylenediamine with

dichloromaleic anhydride, which gave 2,3-dichloropyrrolo[1,2-*a*]benzimidazol-1-one.[8,9] In this paper, we wish to report a comparative study between the reaction of *o*-phenylenediamine with dichloromaleic anhydride and the new reaction of 2,3-diamino-1,4-naphthoquinone with 2,3-dichloromaleic anhydride. particular, we will report a theoretical study employing DFT calculations to understand the electronic structure of the title compound.

RESULTS AND DISCUSSION

Synthesis and crystallization

The reaction of 2,3-dichloromaleic anhydride with *o*-phenylenediamine was reported previously and gave 2,3-dichloropyrrolo[1,2-*a*]benzimidazol-1-one (**2**) without the isolation of the intermediate (**1**),[8] product that looks very attractive as a building scaffold to many derivatives of benzimidazole.[9] According to this result, we carried out the reaction of 2,3-diamino-1,4-naphthoquinone with 2,3-dichloromaleic anhydride under the same reaction conditions used for the previous reaction. No cyclization product, however, to the imidazole ring was isolated; instead, the intermediate product (**3**) was obtained, in which the maleimide ring was formed by the condensation of one amino group of the naphthoquinone with the maleic (Scheme 1). Many attempts were carried out to cyclize **3** to **4**, including refluxing the reaction for a prolonged time (overnight), using different acid catalysts such as (H_2SO_4, *p*-tosylOH, AcOH), changing solvent into AcOH, toluene, DMF or even using the microwave irradiation. No cyclization to the product (**4**) was detected despite the well-known favorable intramolecular cyclization of the amine group with the imide carbonyl group.

The difference in the ease of cyclization between **1** and **3** was expected, and usually was attributed to the low nucleophilicity of the second amine group on the naphthoquinone moiety, due to the presence of many electron-withdrawing groups in its vicinity,[10] and its location on the alpha position of the carbonyl group makes it behave as an amidic like nitrogen.[11] We want, however, to go further and to investigate more the theoretical reason behind this big difference in reactivity between **1** and **3**.

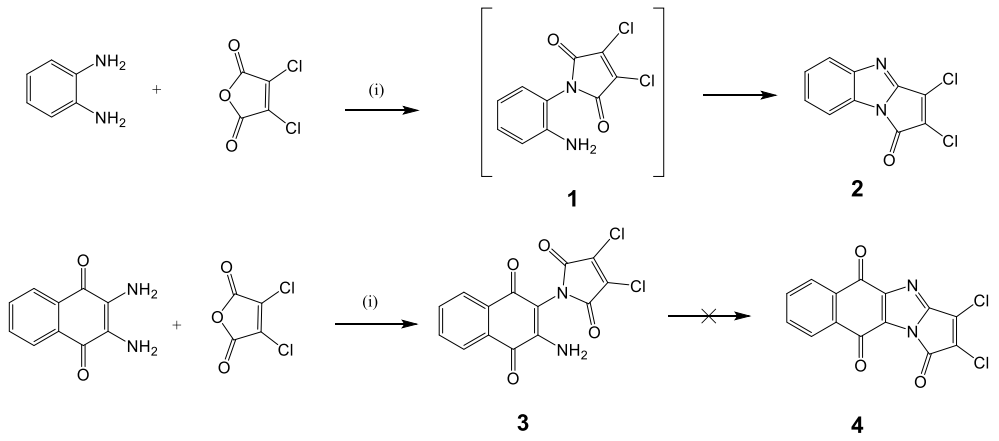

Scheme 1. Reagents and conditions (i): PTSA, toluene, 110 °C

Structural analysis

The neutral complex formed and identified as $C_{14}Cl_2H_6O_4N_2 \cdot C_3D_6O$ crystallizes in the triclinic space group, $P_{\bar{1}}$. As shown in Figure 1, the asymmetric unit contains a single molecule of **3** with deuterated acetone as a crystallization solvent. The averages of (C-O) distances in the quinone and maleic anhydride (C=O) are 1.227 Å and 1.191 Å, respectively. The N-C distance is equal to 1.404 Å and 1.322(4) Å for tertiary and primary amines, respectively, which is equivalent to a single bond. In-ring, all carbon-carbon bond lengths were calculated in the range of 1.390-1.405 Å for 6-311+G(d,p)/B3LYP and observed in the range of 1.370(5)-1.389(4) Å for XRD data. These data can be comparable with literature data. Furthermore, the distance C2–C3 is close to a double bond (1.310(4) Å), while other C-C bond distances are involved in resonance. These distances are in agreement with other similar compounds found in the literature.[8,12] The structure of the compound can be seen as two perpendicular planes with an angle between planes (20 24 146; 2,3-dichloromaleate) and (183 24 419; 2,3-diamino-1,4-naphthoquinonyl) is equal to 104.008°.

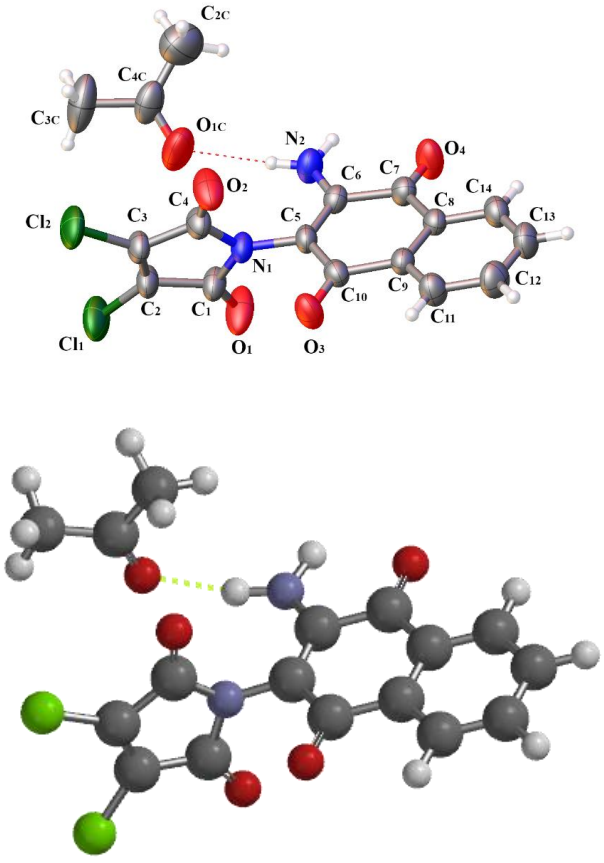

Figure 1. Labeled diagram of the title compound. Displacement ellipsoids were drawn at the 35% probability. Dashed lines show the N-H…O intramolecular hydrogen bonds. (b) The theoretical geometric structure of the title compound at level B3LYP/6-31G(d,p) of theory.

The optimized structure parameters of the title compound were calculated at 6-31G(d,p) and 6-311+G(d,p)/B3LYP level of theory. Selected geometrical parameters of both theoretical and experimental are listed in Table 1.

Table 1. Selected optimized and experimental geometries parameters of the title compound in the ground state.

Bond distance (Å)	CSDX	631G(d,p)	6311+G(d,p)
C_1-C_2	1.493(4)	1.509	1.506
C_2-C_3	1.310(4)	1.341	1.339
C_3-C_4	1.494(4)	1.506	1.505
C_5-C_6	1.363(4)	1.374	1.366
C_5-C_{10}	1.436(4)	1.457	1.460
C_6-C_7	1.507(4)	1.516	1.514
C_7-C_8	1.468(4)	1.477	1.477
C_9-C_{10}	1.490(4)	1.499	1.498
C_8-C_9	1.389(4)	1.407	1.405
C_8-C_{14}	1.387(4)	1.400	1.398
C_9-C_{11}	1.382(4)	1.395	1.393
C_{11}-C_{12}	1.380(4)	1.395	1.393
C_{12}-C_{13}	1.377(5)	1.399	1.396
C_{13}-C_{14}	1.370(5)	1.392	1.390
N_1-C_4	1.397(3)	1.401	1.413
N_1-C_5	1.425(3)	1.424	1.425
N_1-C_1	1.391(3)	1.411	1.413
N_2-C_6	1.322(4)	1.337	1.341
O_1-C_1	1.191(3)	1.204	1.199
O_2-C_4	1.191(3)	1.201	1.199
O_3-C_{10}	1.237(3)	1.231	1.224
O_4-C_7	1.216(3)	1.226	1.219
Cl_1-C_2	1.686(3)	1.710	1.704
Cl_2-C_3	1.689(3)	1.706	1.705
N_2-H_{2A}	0.839	1.020	1.006
N_2-H_{2B}	0.893	1.021	1.010

Bond angle (°)			
N_2-C_6-C_5	125.8(3)	126.59	125.89
N_2-C_6-C_7	114.8(3)	113.69	113.85
C_1-N_1-C_5	124.5(2)	122.36	122.47
C_4-N_1-C_5	125.1(2)	124.10	122.74
C_1-N_1-C_4	110.3(2)	110.55	110.25
N_2-H_{2B}…O_4	2.295	2.162	2.225
Dihedral angle (°)			
C_1-N_1-C_5-C_{10}	75.41		
C_4-N_1-C_5-C_6	79.66		
C_1-N_1-C_5-C_6	-104.13		
C_4-N_1-C_5-C_{10}	-100.80		
Plane-to-plane (°)	55.62	83.9	88.28

Intermolecular interactions and Hirshfeld surface analysis

The crystal structure of **3** is dominated by intra- and intermolecular interactions *i.e.* strong hydrogen bonding -NH_2···O=C(CH_3)$_2$ and medium interaction Cl···O(APD). Moreover, less directional electrostatic attractions between the weak interactions DDDP centroid···O=C(Me)$_2$ are also shown (Figure 2). These intermolecular interactions of DA distances of the N···HO and Cl···O=C hydrogen bonds are shown in Table 2.

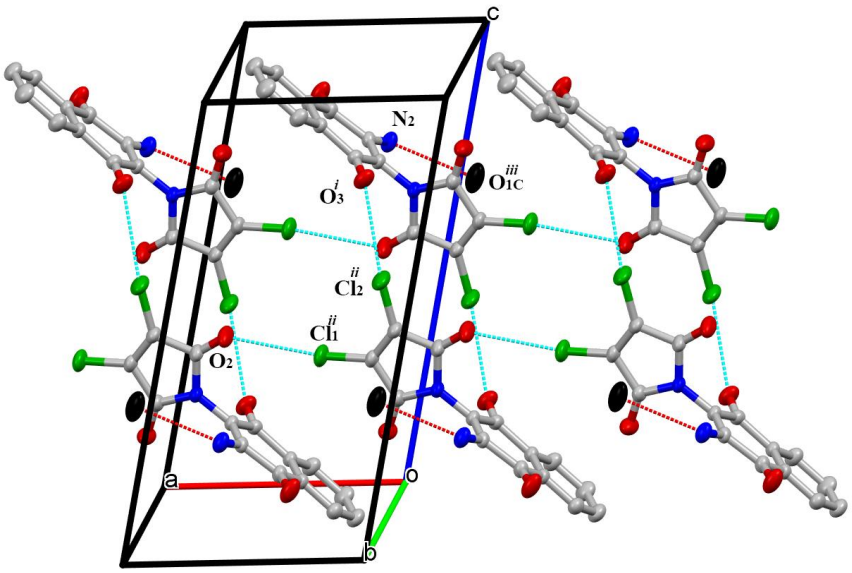

Figure 2. Packing diagram of the title compound showing the different N-H···O and Cl···O=C interactions where *i* = 1-x, 1-y, 1-z, *ii* = 1-x,y,z and *iii* = -x, -y,-1-z. Only the oxygen of the crystallization solvent "acetone" is shown and colored in black.

Table 2. Hydrogen-bond geometry (Å, °)

Donor-H···Acceptor	**D-H**	**H···A**	**D···A**	**D-H···A**
N_2-H_{2A}···O_{1C} *#iv*	0.84(4)	2.08(4)	2.917(4)	172(3)
N_2-H_{2B}···O_3 *#v*	0.90(5)	2.49(5)	3.240(4)	141(3)
N_2-H_{2B}···O_3	0.90(5)	2.30(4)	2.648(4)	103(3)
Cl_1-H_{11}···O_3	0.91(3)	2.51(3)	2.817(4)	100(2)
Cl_1-H_{11}···O_4 *#vi*	0.91(3)	2.57(3)	3.336(5)	143(3)

Symmetry codes: iv = 1+x, 1+y, z; v = x, 1+y, z; vi = x, -1+y, z

The interaction energy between the crystallization solvent (acetone) and **3** can be expressed as the energy difference between the whole system and its subunits, each evaluated at their geometries on their own basis sets. To compute the correct value of the interaction energy, we need to use basis set superposition error (BSSE) as a full counterpoise method.[13] To confirm the reliability of calculated results, DFT with hybrid B3LYP functional, M06, and EDF2 methods were chosen, and the effect was estimated using bases set 6-31G(d) and 6-31G(d,p). The corresponding interaction energies, corrected with the BSSE are listed in Table 3. The EDF2 and B3LYP results were in reasonable agreement with the MP2, and no great difference was shown when a higher basis set (6-31G(d,p) was used.

Table 3. Interaction (CP) (kJ/mol) calculated by several methods and basis sets

Basis set/ Method	B3LYP	M06	EDF2	MP2
6-31G(d)	-15.776	-32.628	-20.581	-26.992
6-31G(d,p)	-15.694	-32.942	-20.515	-26.995

Hirshfeld Surface Analysis

Hirshfeld surfaces[14] and the associated 2D-fingerprint plots[15] of the title molecular salt have been generated using Crystal Explorer 17.[16] Hirshfeld surfaces mapped with different properties; d_{norm}, shape index, and curvedness, have proven to be a useful visualization tool for the analysis of intermolecular interactions. 2D-Fingerprint plots of Hirshfeld surfaces presented the different intermolecular interactions percentages. Hirshfeld surface analysis of **3** (without crystalline water), as specified in Figure 3. 2D-Fingerprint plots are showing contributions from different contacts: (a) overall interactions (b) CH/HC (c) CO/OC (d) HH (e) NH/HN (f) OH/HO (g) NO/ON are depicted in Figure 4 and demonstrates that the OH/HO dominate in the crystal with 26% of the total interactions.

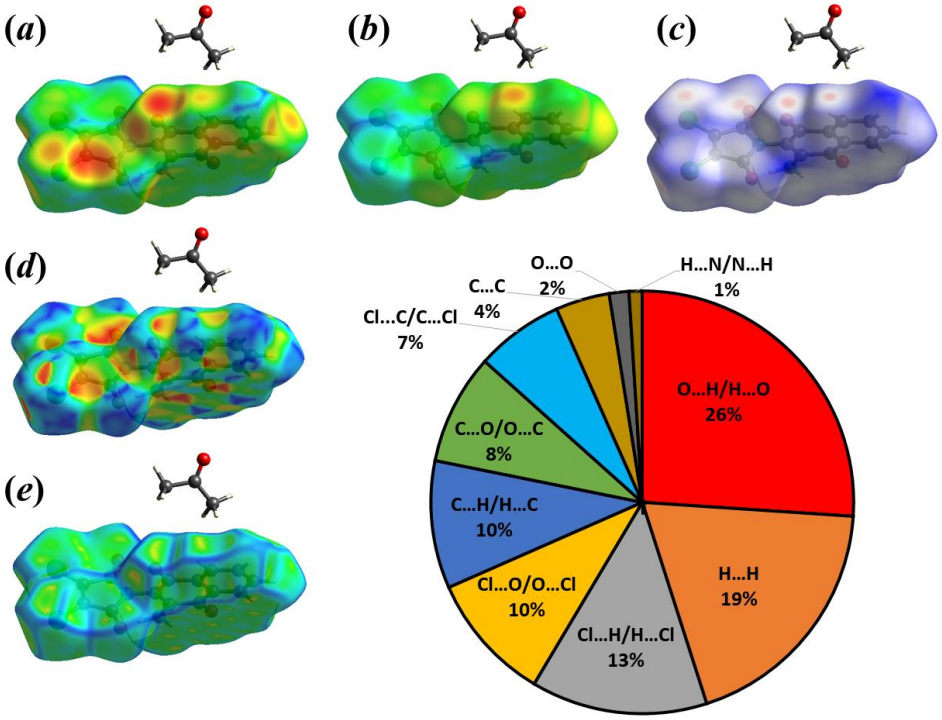

Figure 3. 3D Hirshfeld surface analysis of **3** mapped over (a) shapeindex, (b) curvedness, and (c) d_{norm} and a pie chart showing the percentage of intermolecular interactions distribution in **3**.

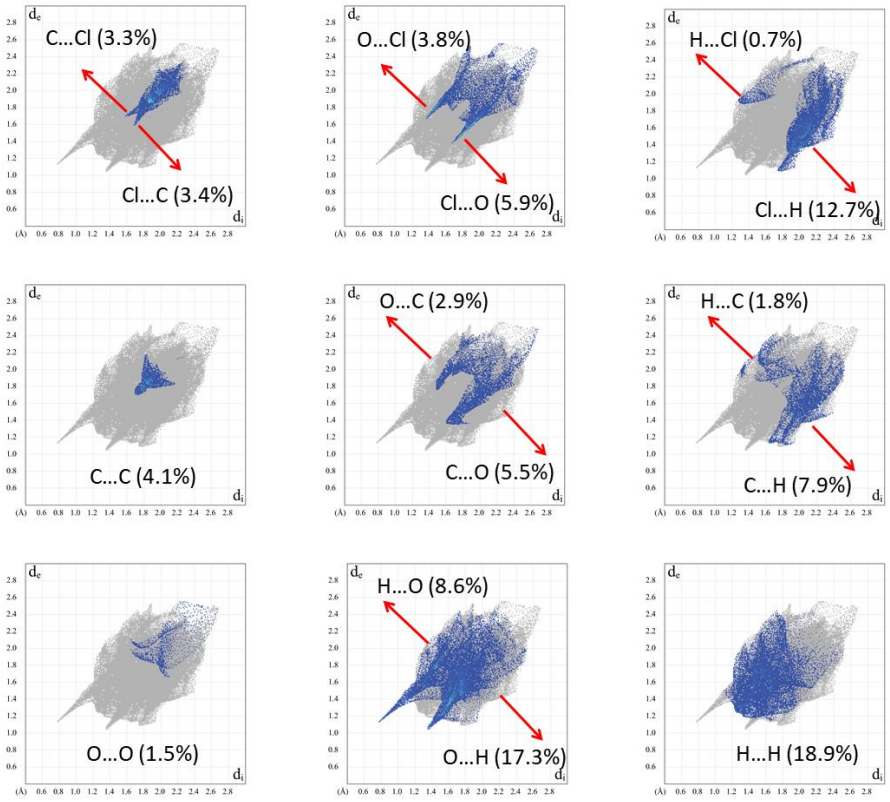

Figure 4. 2D-Fingerprint plots showing contributions from different contacts

Charge

To gain insight into the reason for no cyclization to the imidazole ring **4**, we firstly proposed a hypothesis that is intermolecular interaction with the crystallization solvent (acetone). We probed the reaction in more detail, computationally. The natural charges were calculated at B3LYP/6-31G(d,p) level of calculation (Figure 5).

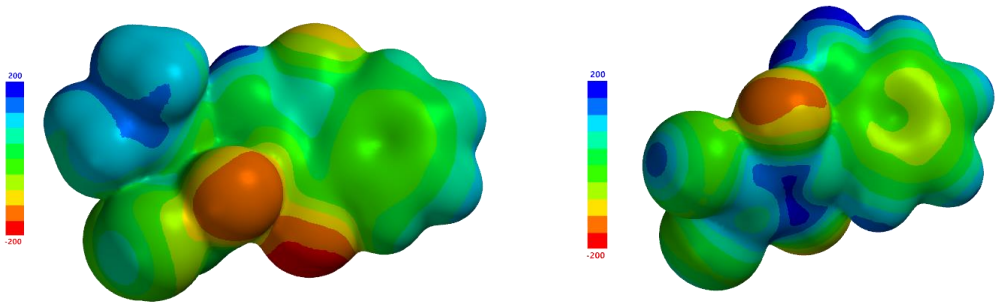

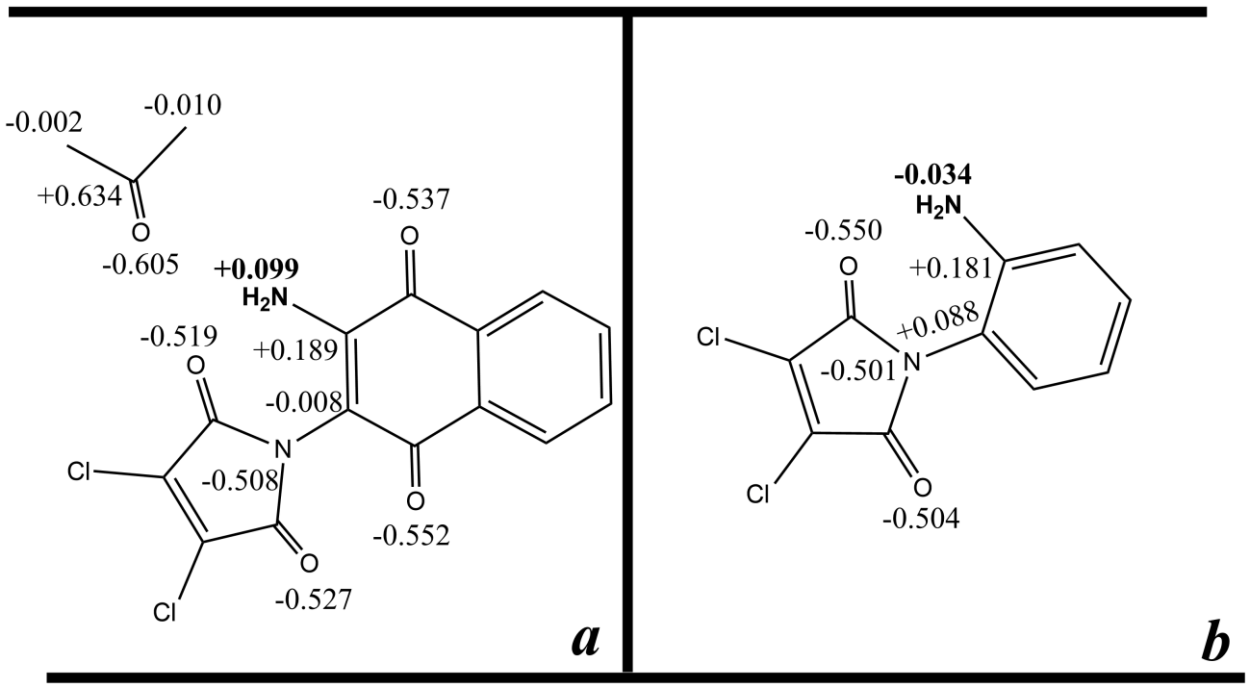

Figure 5. Above) Electrostatic surface potential (ESP) for the **3** and **1**, respectively. Below) the main charge calculated B3LYP/6-31G(d,p) level of calculation for (a) **3** and (b) **1**.

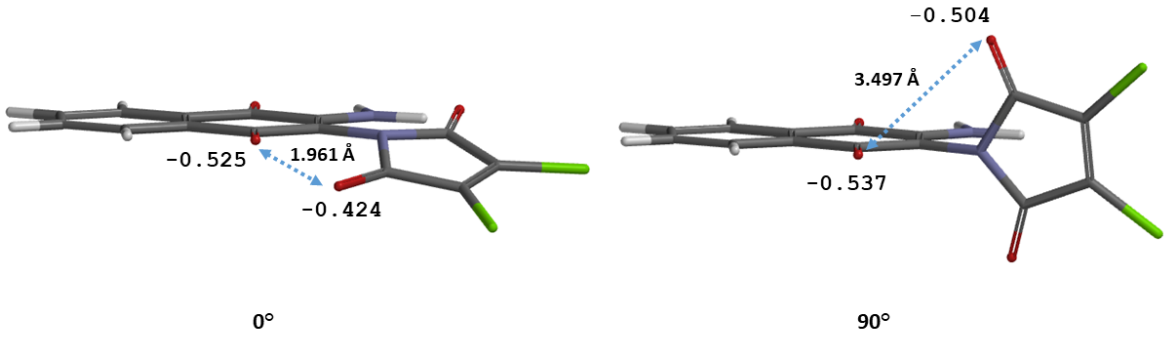

Figure 6. Different views at a hypothetical angle 0° and 90° and the calculated charges for both cases

According to these calculations, the carbon connected to the amine (NH_2) group in **3** is much more electrophilic than that connected to the maleimide ring, which resulted in reducing the nucleophilicity of the attached amino group. The electron density calculation on the amine group reveals that the amine carries a positive charge instead of the expected negative charge, results that may explain the failure of cyclization compared with its phenyl analogous **1**. As we can see from the potential electronic surface (EPS) plotted on the isodensity surface for **1**. In Figure 5, it is shown that the positive surface is concentrated on the crystallization solvent. The main interaction is between the amine and the oxygen of crystallization solvent acetone. Moreover, Figure 6 shows the charges on both oxygen atoms on the maleimide and naphthoquinone moieties and the distances between them in both cases where the dihedral

angles are 0° and 90°. For the ring cyclization to take place, both rings should be nearly coplanar, a fact that reduces the distance between the two negatively charged oxygen atoms and makes the repulsion between them even higher. Thus, we believe that the failure of the cyclization of **3** to the imidazole ring could be attributed to both factors, the low nucleophilicity of the nitrogen atom and the high repulsion between both oxygen atoms.

HOMO and LUMO analysis

The calculations indicate that the compound has 85 occupied molecular orbitals (MOs). Figure 7 shows the distributions and energy levels of the HOMO and LUMO orbitals computed at the B3LYP/6-31G (d,p) level for the title compound. The analysis of the wave function obtained by B3LYP/6-31G (d,p) indicates that the electron absorption corresponds to the transition from the ground state to the first excited state and is mainly described by the one-electron excitation from the HOMO to the LUMO (Figure 7).

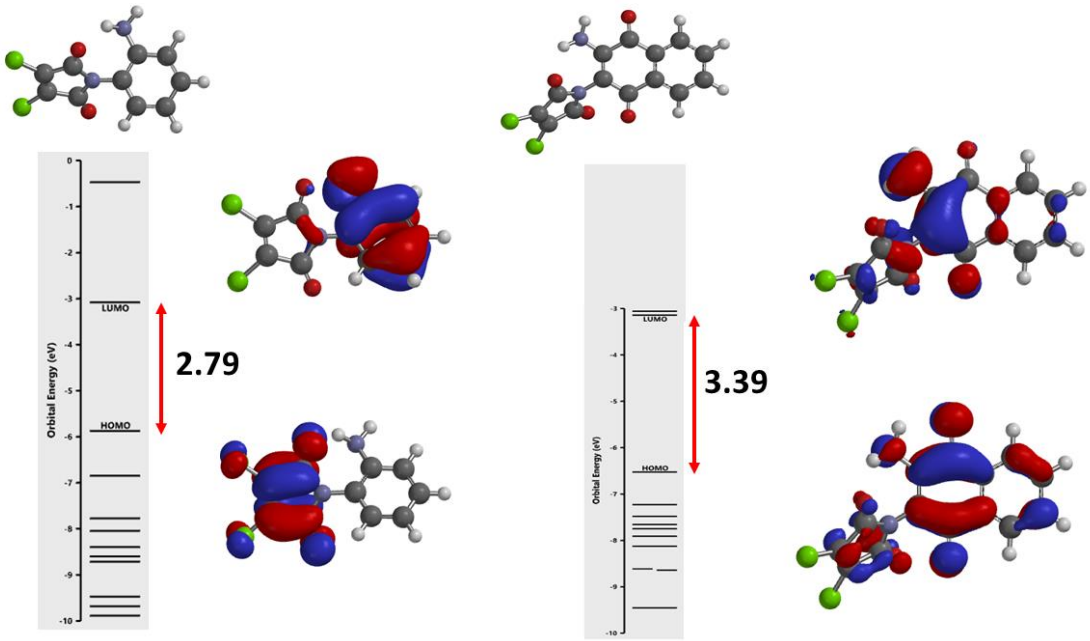

Figure 7. The frontier MOs with energy gap labels of **1** and **3**, respectively. Only HOMO and LUMO are drawn.

The HOMO-LUMO gap is associated with the stability and reactivity of a chemical system. The larger the energy gap, the harder and more stable and less reactive the molecule and *vice versa*. As seen in Figure 7, the gaps of **1** and **3** are 2.79 and 3.39, respectively. This difference in the energy gap means that the stability of **1** is less than **3**, and its ring can be closed easier.

The HOMO of **3** is delocalized over the C-C bond in the quinone part of the naphthoquinone moiety and on the lone pair of the amine. By contrast, the LUMO is located over the C=C of the aromatic part of the quinone. Furthermore, the HOMO-LUMO in **3** transition implies an electron density transfer inside the quinone ring. The LUMO energies in both cases are almost the same, and this makes using HOMO as a unique frontier orbital is possible. The HOMO on aminophenyl part in **1** is null in comparison with the malemaide in contrast of **3** where the HOMO is spread over the amine, which makes it harder to close the ring in **3**. In the case of **1**, the higher value of HOMO energy of a molecule tends to donate electrons to an appropriate acceptor molecule with low energy, empty molecular orbitals.

CONCLUSION

Compound $C_{14}Cl_2H_6O_4N_2 \cdot C_3D_6O$ (**3**$\cdot C_3D_6O$) has been synthesized, and its crystal structure was solved by a single-crystal X-ray diffraction method. The geometries were optimized using DFT at 6-311+G(d,p)/B3LYP and 6-31G(d,p)/B3LYP method level of theory and is comparable to the experimental structure obtained by single-crystal structure. The most stable optimized geometries at a local energy minimum were verified and showed a lack of any imaginary vibrational frequency. The energy of interaction between the **3** and the crystallization solvent (C_3D_6O) was calculated by various methods M06/MP2/EDF2 with 6-31G(d), and 6-31G(d,p) basis sets and the obtained energy was corrected by basis set superposition errors (BSSE). The reactions of *o*-phenylenediamine and 2,3-diamino-1,4-naphthoquinone with 2,3-dichloromaleic anhydride which afforded to the intramolecular cyclization to the fused imidazole in the first case but failed to cyclize to the imidazole in the second case. The failure in cyclization could be attributed to the low nucleophilicity of the amine in addition to the repulsion between both negatively charged oxygen atoms in the naphthoquinone and the maleimide moieties. Finally, the frontier orbitals (HOMO-LUMO) confirms the stability in the case of **3** that make the cyclization in its case to be failed.

EXPERIMENTAL

Materials and methods

All chemicals were commercially purchased and used without further purification. The ^{1}H NMR spectra were recorded on a Bruker Avance III-400 MHz spectrometer with TMS as an internal standard and the ^{13}C NMR spectra at 100 MHz using a Bruker Avance III-400 MHz spectrometer with TMS as an internal standard. Chemical shifts are reported as δ-values in ppm. Spectra were acquired in acetone-d_6. High-resolution mass spectra (HRMS) were recorded in positive ion mode by electrospray ionization using a Bruker Daltonics Apex IV, 7.0 T Ultra Shield Plus (Bremen, Germany). The samples were dissolved in chloroform, diluted in spray solution (MeOH/water 1:1 *v/v* + 0.1% formic acid), and infused

using a syringe pump with a flow rate of 2 μL/min. External calibration was conducted using the arginine cluster in a mass range *m/z* from 175-871. HRMS data were recorded at mass error: 0.00 – 0.50 ppm. Melting points (mp) were determined on an electrothermal melting point apparatus and are uncorrected. Solvents used in this study were obtained from Scharlau, Fluka, and Aldrich. All reactions were monitored by thin-layer chromatography (TLC) using Merck aluminum plates pre-coated with silica gel PF254 (20 × 20 × 0.25 mm) and detected by visualization of the plate under UV lamp (λ = 254 or 365 nm). Spots were also detected by spraying with anisaldehyde- sulphuric acid in ethanol, followed by heating to 140 °C.

Preparation of 1-(3-amino-1,4-dioxo-1,4-dihydronaphthalen-2-yl)-3,4-dichloro-1*H*-pyrrole-2,5-dione (3)

To 100 mg (0.60 mmol) of 2,3-dichloromaleic anhydride and 113 mg (0.60 mmol) of 2,3-diamino-1,4-napthoquinone in a reflux apparatus equipped with a Dean-Stark trap was added 10 mL of toluene and 10 mg of PTSA. The reaction was heated at 110 °C for 3 h and then allowed to cool to room temperature. The toluene was removed under vacuum. The residue was purified by column chromatography using CH_2C1_2 as the eluent. Yield 112 mg (56%). IR: $\bar{\upsilon}$ = 3390, 3629 (NH_2), 1828 C=O, 1704, 1453 cm^{-1}. ^1H NMR (400MHz, acetone-d_6): 7.21 (bs, 1H, NH), 7.42 (bs, 1H, NH), 7.87 (m, 2H), 8.12 (m, 2H). ^{13}C NMR (100 MHz): 169.1, 161.9, 148.8, 135.3, 133.9, 132.9, 132.3, 130.6, 126.5, 126.1. HRMS (ESI) *m/z* : calculated for $C_{14}H_6Cl_2N_2O_4Na$ $[M+Na]^+$ = 358.9602, found 358.9621.

X-Ray crystallographic measurements

Single-crystals of $C_{14}Cl_2H_6O_4N_2 \cdot C_3D_6O$ were collected with the aid of an Oxford Diffraction Xcalibur (Mo) X-ray source (λ = 0.71073 Å) at 293 ± 2 K. Collection and reduction of data, as well as cell refinement, were performed with the CrysAlisPro software package.[17] The crystal was kept at 293(2) K during data collection. Using Olex2,[18] the structure was solved with the ShelXS[19] structure solution program using Direct Methods and refined with the ShelXL[19] refinement package using Least Squares minimization. All hydrogen atoms were found *via* Fourier difference maps. Further, the hydrogen on nitrogen and water were located by Fourier difference and refined isotopically, CH_3 atoms were refined with riding coordinates. Mercury program is used for the crystal structure plotting. The crystals data have been deposited at the Cambridge Crystallographic Data Center CCDC-2005769. Crystal data and structural refinements are listed in Table 4.

Table 4. Crystal data and structure refinements for **3**

Empirical formula	**$C_{17}H_{12}Cl_2N_2O_5$**
Formula weight	395.19
Temperature/K	293(2)
Crystal system	triclinic
Space group	P_{-1}
a/Å	7.8792(15)
b/Å	7.9415(15)
c/Å	14.774(3)
α/°	104.122(18)
β/°	102.195(18)
γ/°	95.375(18)
Volume/Å^3	865.9(3)
Z	2
ρ_{calc} g/cm^3	1.516
μ/mm^{-1}	0.407
F(000)	404.0
Crystal size/mm^3	0.7658 × 0.4223 × 0.2609
Radiation	MoK_α ($\lambda = 0.71073$)
2Θ range for data collection/°	6.764 to 50.042
Index ranges	$-9 \le h \le 9$, $-9 \le k \le 9$, $-17 \le l \le 17$
Reflections collected	5574
Independent reflections	3055 [$R_{int} = 0.0246$, $R_{sigma} = 0.0521$]
Data/restraints/parameters	3055/0/261
Goodness-of-fit on F^2	1.035
Final R indexes [I ≥ 2σ (I)]	$R_1 = 0.0532$, $wR_2 = 0.1149$
Final R indexes [all data]	$R_1 = 0.0789$, $wR_2 = 0.1321$
Largest diff. peak/hole / e Å^{-3}	0.38/-0.41

Computational details

All methods were within the program Spartan version'04. The geometries were optimized and compared with the crystal structure obtained by X-ray (CSDX). The most stable optimized geometries at a local energy minimum were verified by the lack of any imaginary vibrational frequency. The optimized and molecular energies, charge, and vibrational frequencies of the $C_{14}C_{l2}H_6O_4N_2 \cdot C_3D_6O$ compound were calculated using the 6-31G(d,p) and 6-311+G(d,p)/B3LYP method. The energy of interaction between two molecules A and B in dimer or complex AB was calculated by various methods M06/MP2/EDF2 with 6-31G(d) and 6-31G(d,p) basis set as $\Delta E = E(AB) - E(A) - E(B)$, where E denotes electronic energies of respective species. ΔE were corrected to account for basis set superposition errors (BSSE) that ensures the simultaneous optimization of geometries of dimeric complexes along with their components and hence overcome the superposition.

ACKNOWLEDGEMENTS

We wish to thank The Hashemite University for financial support.

REFERENCES

1. Y. Bansal and O. Silakari, *Bioorg. Med. Chem.*, 2012, **20**, 6208.
2. P. Zhan, D. Li, J. Li, X. Chen, and X. Liu, *Mini-Rev. Org. Chem.*, 2012, **9**, 397.
3. M. Gaba, S. Singh, and C. Mohan, *Eur. J. Med. Chem.*, 2014, **76**, 494.
4. A. A. El Rashedy and H. Y. Aboul-Enein, *Mini-Rev. Med. Chem.*, 2013, **13**, 399.
5. A. A.El Rashedy and H. Y. Aboul-Enein, *Curr. Drug Ther.*, 2013, **8**, 1.
6. J. M. Miguel del Corral, M. A. Castro, M. Gordaliza, M. L. Martin, A. M. Gamito, C. Cuevas, and A. S. Feliciano, *Bioorg. Med. Chem.*, 2006, **14**, 2816.
7. V. K. Tandon, D. B. Yadav, H. K. Maurya, A. K. Chaturvedi, and P. K. Shukla, *Bioorg. Med. Chem.*, 2006, **14**, 6120.
8. W. H. Watson, G. Wu, and M. G. Richmond, *J. Chem. Crystallogr.*, 2004, **34**, 757.
9. B. A. Salameh, H. Mahmoud, M. A. Khanfar, and R. A. Al-Qawasmeh, *J. Heterocycl. Chem.*, 2019, **56**, 1530.
10. B. A. Salameh, R. A. Al-Qawasmeh, K. Al-Jabari, and W. Voelter, *Res. Chem. Intermed.*, 2015, **41**, 2929.
11. A. J. Hamdan and S. Al-Jaroudi, *Arab. J. Sci. Eng.*, 2003, **28**, 51.
12. S. A. Matar, W. H. Talib, M. S. Mustafa, M. S. Mubarak, and M. A. AlDamen, *Arab. J. Chem.*, 2015, **8**, 850.
13. S. Simon, M. Duran, and J. J. Dannenberg, *J. Chem. Phys.*, 1996, **105**, 11024.

14. M. A. Spackman and D. Jayatilaka, *CrystEngComm*, 2009, **11**, 19.
15. J. J. McKinnon, D. Jayatilaka, and M. A. Spackman, *Chem. Commun.*, 2007, **37**, 3814.
16. M. J. Turner, J. J. McKinnon, S. K. Wolff, D. J. Grimwood, P. R. Spackman, D. Jayatilaka, and M. A. Spackman, *CrystalExplorer17*. The University of Western Australia Perth, WA, Australia 2017.
17. Agilent, P. R. O. CrysAlis, Agilent Technologies, Yarnton, Oxfordshire, England, 2011.
18. O. V. Dolomanov, L. J. Bourhis, R. J. Gildea, J. A. K. Howard, and H. J. Puschmann, *J. Appl. Crystallogr.*, 2009, **42**, 339.
19. G. M. Sheldrick, *Acta Crystallogr. A*, 2008, **64**, 112.
20. F. B. van Duijneveldt, J. G. C. M. van Duijneveldt-van de Rijdt, and J. H. van Lenthe, *Chem. Rev.*, 1994, **94**, 1873.